

# Design and analysis of trans Z-source inverter for electric vehicle applications using neural network-clustering

Manish Bharat<sup>1,3</sup>, ASR Murty<sup>2</sup>, Ritesh Dash<sup>3</sup>

<sup>1</sup>Department of Electrical and Electronics Engineering, Visvesvaraya Technological University, Belagavi, India

<sup>2</sup>Department of Electrical and Electronics Engineering, Rajarajeswari College of Engineering, Bengaluru, India

<sup>3</sup>School of Electrical and Electronics Engineering, REVA University, Bengaluru, India

## Article Info

### Article history:

Received Sep 18, 2022

Revised Nov 8, 2022

Accepted Dec 21, 2022

### Keywords:

Electric vehicle

Quasi-Z-source

Total harmonic distortion

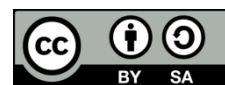
Trans Z source

Z-source inverter

## ABSTRACT

The presented paper analyzes the detailed design of a trans Z-source inverter (ZSI) with an input from solar photovoltaic (SPV) system. Increase in SPV uses requires highly efficient SPV enabled inverters under varying weather parameters are in high demand in modern smart grid applications. The SPV-trans ZSI has high conversion efficiency because of the single-stage voltage boost conversion capability. In contradiction, the conventional voltage source inverter (VSI) requires an additional step-up transformer to boost the output voltage of inverter. This reduces the efficiency by increasing the volume of set up and also increase the cost of the system. In the proposed SPV system it provides a better output against VSI. The increase in inverter output voltage is because of shoot through time period present in ZSI. It also reduces the voltage stress and harmonics content as compared to VSI. The proposed model has been validated through MATLAB simulation.

*This is an open access article under the [CC BY-SA](https://creativecommons.org/licenses/by-sa/4.0/) license.*



## Corresponding Author:

Manish Bharat

School of Electrical and Electronics Engineering, REVA University

Bengaluru, India

Email: manishb87@gmail.com

## 1. INTRODUCTION

These days, it is noticed that renewable energy resources like solar energy and power from wind energy have been extensively find its application in energy to mitigate the ever increase in demand of the clean and green electrical energy. Again from the literature studies it can be found that solar photovoltaic (SPV) system drags the attention of global researcher's to meet the present energy requirement. In case of SPV generating system, inverter represents an important part. In traditional conversion system, in order to increase the voltage level DC-DC boost converter or transformer is generally used. This in turn increases the power losses present in the inverter and also increases the overall cost of system. Increase in conversion stage reduce the efficiency of the system.

A remarkable voltage step change for a single-stage conversion can be possible through a Z-source inverter (ZSI), where a high impedance network is used before the voltage source inverter (VSI) circuit. Again from the literature survey many topologies in this field can be found. A modified efficient boost, low cost and a low voltage loss for impedance source inverter was analyzed. A detailed derivation and analysis of ZSI under the quasi-Z-source inverter (q-ZSI), representing different configurations, while retaining the operating principle was discussed at ref [1], [2]. The advantages present in q-ZSI against ZSI is of low device rating, filtering capacitor less, less ripples in switching interval and maintains an constant DC ripple free input current to the inverter circuit from SPV [3], [4].

A typical electric vehicle (EV) consists of motors, battery, battery management system, DC to DC converter and DC to AC converter supporting components to transmit the power from battery to the electric motors. Parameter seizing in an electrical vehicle is the most important task because of the use of power electronic components and switches which requires precise operation of frequency for smooth and continuous operation. Again from the operation and control point of view synchronous motor or induction motor is basically used in EV application which will also reduce the overall cost of the EV. The typical operation features that include in induction motor are speed control over a wide range of variation can be achieved with minimum time, DC to AC converter design it's simple and robust which leads to less maintenance cost [5], [6].

A typical induction motor requires high starting torque and large amount of power is required at the initial stage. During hill climbing the torque requirement for the induction motor to drive is very high which leads to increase in power density, this sometimes requires fast torque response during emergency braking operation. Therefore regenerative braking with high efficiency in conversion ratio is a required parameter for successful operation of the EV induction motor [7], [8].

Battery power EV are the most prominent and advanced architecture for powering the induction motor in the EV. This requires a conversion of DC to DC and from DC to AC before applying to the induction motor. The variation in the EV speed during acceleration and retardation leads to the variation in the current drawn from the converter [9]–[11]. This also increases the switching stress on the different power electronic components and thereby affecting the battery discharge rate. With the advancement in the inverter circuit a number of research is going on regarding reduction of switching stress during acceleration and retardation situation. It is understood that from the literature survey, ZSI can be utilised because of some technical advantages as well as reduction in the number of conversion stages [12]–[14].

This paper presents a detailed analysis of different types of Z source converter and their applications in the EV for power transmission from battery to the induction motor drive. A new topology for ZSI has been presented under section 3 along with its block diagram and control method. The validation of the system has been carried out with MATLAB/Simulink model along with experimental analysis for a 5 KW induction motor. It is observed that the proposed model not only increases the efficiency of the EV but also reduces the overall cost in terms of switching stress and its components in use. Due to one stage conversion of the system the overall efficiency of the inverter is also increased along with easy implementation in its control algorithm [15], [16].

## 2. Z-SOURCE INVERTER IN AUTOMOTIVE APPLICATION

### 2.1. Quasi-Z-source inverter

In multilevel inverter, with increase in switching frequency, the switching losses also increases and hence the total loss present in multilevel inverter can be treated as a function of switching frequency. According to the literature survey as presented under section 1, the switching loss can be reduced by two methods, such as zero current switching or zero voltage switching and selective harmonics elimination by using space vector pulse width modulation (PWM). In this section q-ZSI with dual input is received from battery and SPV has been model to fed two different ac loads in the EV application. In order to strategies the concept, multilevel inverter has been considered over here [17], [18].

In this paper an extended version of q-ZSI as shown in Figure 1 with two source, 9 switches and bidirectional switches between the source and the load has been designed. The basic architecture of the stated model has been shown in Figure 1 and Figure 2. In Figure 1 continuous current conduction mode with two voltage sources has been presented whereas in Figure 2 discontinuous current conduction mode with voltage fed source has been presented. The stated q-ZSI can provide the buck boost operation while transforming input to output [19], [20]. In order to improve the efficiency by reducing the switching losses at higher switching frequency is the primary requirement for EV applications. Here sinusoidal PWM has been applied by considering the concept of no switching zone of 60 degree when the load is at the peak of voltage and fundamental current [21].

In continuation to the about control strategy, the control scheme consisting of a combination of two sine waves and two triangular wave has been used on per basis for 9 different switches in a synchronize manner. As a practice of the PWM generation techniques top a triangular wave need to be compared with open sine wave and that's off the lower triangular wave needs to be compared with lower sine wave. In the q-ZSI, three different modes of conduction can be achieved by arranging the frequency content of sinusoidal waveform viz - a viz the shoot through mode can be achieved by maintaining a frequency of sinusoidal envelope at three times as compared to the modulating sinusoidal signal. The shoot through mode can be applied if the upper triangular wave is less the lower sinusoidal wave. Depending upon the above condition S1 and S7 can be turned on. In order to achieve a proper three phase voltage at the output of load 1, the XOR pulse of S1 and S7 has been applied to S4 [22], [23].

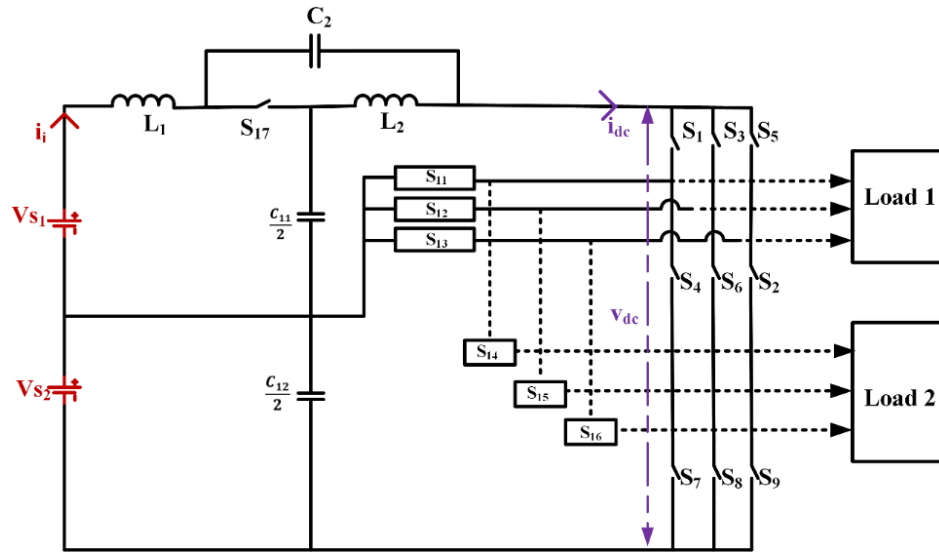


Figure 1. q-ZSI connected to critical load and non-critical load

In contradiction S10 and S13 will be the NOR signal of the signal that is applied to S1 and S7. During the shoot through state S1 to S9 are closed making the multilevel inverter full dead short circuit. As part of the q-ZSI, S10 to S15 are made open for generating the voltage across the capacitor [24], [25]. The state space model for the q-ZSI can be analysed considering three modes of operation such as active voltage mode, shoot through mode and zero voltage mode for capacitor voltage, load current and inductance current can be presented as follows:

$$\frac{d}{dt} \begin{pmatrix} \frac{\Delta i_{L1}}{s} \\ \frac{\Delta i_{L2}}{s} \\ \frac{\Delta v_{C11}(s) + \Delta v_{C12}(s)}{2} + \frac{\Delta v_{C2}(s)}{2} \end{pmatrix} \begin{pmatrix} -\frac{1}{L_1(s)} & 0 & \frac{(d-1)}{L_1(s)} & \frac{d}{L_1(s)} \\ 0 & -\frac{1}{L_2(s)} & \frac{d}{L_2(s)} & \frac{(d-1)}{L_2(s)} \\ \frac{(1-d)(s)}{C_{11}+C_{12}} & \frac{d(s)}{C_{11}+C_{12}} & 0 & 0 \\ \frac{d(s)}{C_2} & \frac{(1-d)(s)}{C_2} & 0 & 0 \end{pmatrix} \begin{pmatrix} \frac{\Delta i_{L1}}{s} \\ \frac{\Delta i_{L2}}{s} \\ \frac{\Delta v_{C11}(s) + \Delta v_{C12}(s)}{2} + \frac{\Delta v_{C2}(s)}{2} \end{pmatrix} \begin{pmatrix} -\frac{1}{L_1(s)} & (1-d) \\ 0 & (1-d) \\ 0 & (d-1) \\ 0 & (d-1) \end{pmatrix} \begin{pmatrix} \Delta V_{s1}(s) + \Delta V_{s2}(s) \\ i_{dc} \end{pmatrix} \quad (1)$$

$$\begin{pmatrix} \frac{\Delta i_1}{s} \\ \Delta v_{dc}(s) \end{pmatrix} = \begin{pmatrix} 1 & 0 & 0 & 0 \\ (1-d) & (1-d) & (1-d) & (1-d) \end{pmatrix} \begin{pmatrix} \frac{\Delta i_{L1}}{s} \\ \frac{\Delta i_{L2}}{s} \\ \frac{\Delta v_{C11}(s) + \Delta v_{C12}(s)}{2} + \frac{\Delta v_{C2}(s)}{2} \end{pmatrix} \quad (2)$$

Finally, the state-space-averaging (SSA) model of QZSI is expressed:

$$\frac{d}{dt} \begin{pmatrix} \frac{\Delta i_{L1}}{s} \\ \frac{\Delta i_{L2}}{s} \\ \frac{\Delta v_{C11}(s) + \Delta v_{C12}(s)}{2} + \frac{\Delta v_{C2}(s)}{2} \end{pmatrix} = \begin{pmatrix} -\frac{1}{L_1(s)} & 0 & \frac{(D-1)}{L_1(s)} & \frac{D}{L_1(s)} \\ 0 & -\frac{1}{L_2(s)} & \frac{D}{L_2(s)} & \frac{(D-1)}{L_2(s)} \\ \frac{(1-D)(s)}{C_{11}+C_{12}} & \frac{D(s)}{C_{11}+C_{12}} & 0 & 0 \\ \frac{D(s)}{C_2} & \frac{(1-D)(s)}{C_2} & 0 & 0 \end{pmatrix} \begin{pmatrix} \frac{\Delta i_{L1}}{s} \\ \frac{\Delta i_{L2}}{s} \\ \frac{\Delta v_{C11}(s) + \Delta v_{C12}(s)}{2} + \frac{\Delta v_{C2}(s)}{2} \end{pmatrix} \begin{pmatrix} -\frac{1}{L_1(s)} & \frac{(1-D)}{L_1(s)} \\ 0 & \frac{(1-D)}{L_2(s)} \\ 0 & \frac{(D-1)s}{C_1} \\ 0 & \frac{(D-1)s}{C_2} \end{pmatrix} \begin{pmatrix} \Delta V_{s1}(s) + \Delta V_{s2}(s) \\ i_{dc} \end{pmatrix} + \begin{pmatrix} \frac{V_1(s)}{L_1(s)} \\ \frac{V_1(s)}{L_2(s)} \\ \frac{I_1(s)^2}{C_{11}+C_{12}} \\ \frac{I_1(s)}{C_2} \end{pmatrix} (\Delta d) \quad (3)$$

$$\begin{pmatrix} \frac{\Delta i_i}{s} \\ \Delta v_{dc}(s) \end{pmatrix} \begin{pmatrix} 1 & 0 & 0 & 0 \\ (1-D) & (1-D) & (1-D) & (1-D) \end{pmatrix} \begin{pmatrix} \frac{\Delta i_{L1}}{s} \\ \frac{\Delta i_{L2}}{s} \\ \frac{\Delta v_{C11}(s)}{2} + \frac{\Delta v_{C12}(s)}{2} \\ \Delta v_{C2}(s) \end{pmatrix} + \begin{pmatrix} 0 & 0 \\ 0 & -2(1-D) \end{pmatrix} \begin{pmatrix} \Delta V_{s1}(s) + \Delta V_{s2}(s) \\ i_{dc} \end{pmatrix} + \begin{pmatrix} 0 \\ V_2 \end{pmatrix} (\Delta d) \quad (4)$$

where:  $D$  is duty cycle in steady state,  $V_1 = v_{C11} + v_{C12} + v_{C2}$ ,  $I_1 = i_{dc} - i_{L1} - i_{L2}$ ,  $V_2 = -V_1 + I_1$ ,  $X_z = \left[ \frac{\Delta i_{L1}}{s} \quad \frac{\Delta i_{L2}}{s} \quad \frac{\Delta v_{C11}(s)}{2} + \frac{\Delta v_{C12}(s)}{2} \quad \Delta v_{C2}(s) \right]^T$  and  $U_{1z} = [\Delta V_{s1}(s) + \Delta V_{s2}(s) \quad i_{dc}]^T$ ,  $v_{dc}i_{dc} = v_d i_d + v_q i_q = V_{dc} \Delta i_{dc} + I_{dc} \Delta v_{dc} = V_d \Delta i_d + I_d \Delta v_d + V_q \Delta i_q + I_q \Delta v_q$ . Here, Figure 2 represents the q-ZSI connected to critical load and non-critical load where Figure 2(a) represents non-shoot through mode of operation and Figure 2(b) represents the shoot through mode of operation.

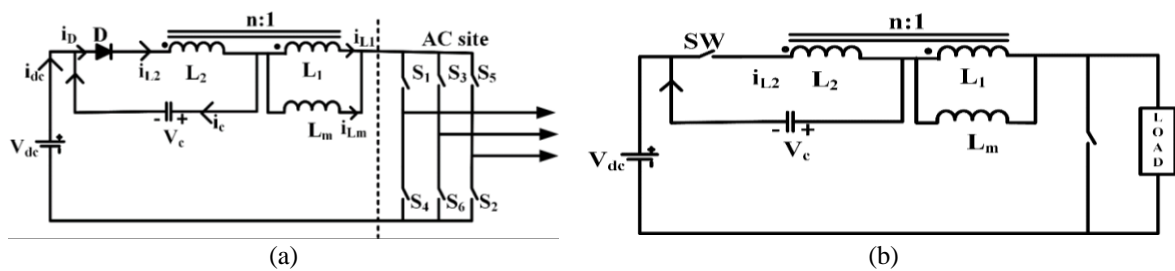


Figure 2. q-ZSI connected to critical load and non-critical load (a) non-shoot through mode and (b) shoot through mode

## 2.2. Embedded Z-source inverter

In shoot through mode the sudden flow of current will increase the power interruption. This also induces power interruptions if the input supply is from SPV. This jumping of current from one state to another state during shoot through mode increase the control complexity and thereby increase the system burden. The increase in complexity is due the high frequency operation of switches and flow of current through the diode. In ZSI the effect can be minimised by placing a inductors and capacitors (LC) filter before the diode. However, the introduction of additional filter at the input side not only increases the complexity but also increases the cost of the system. Presence of LC filter at the input of ZSI will change the dynamics and also introduces resonance at the fundamental frequency [26].

In order to avoid the above issue embedded ZSI has been developed where implicit source filtering at centre frequency can be achieved closely retain the property of ZSI. As a matter of implicit design, it produces turn output with smaller ripple of input voltage and current. Figure 3 represents embedded ZSI, where the analysis can be carried out by assuming the ideality of the all elements and ignoring the dead time present in the pulses. In addition two statement, high capacitance value is considered for the input circuit. Three operating modes based on the shoot through duty cycle of the inverter has been considered.

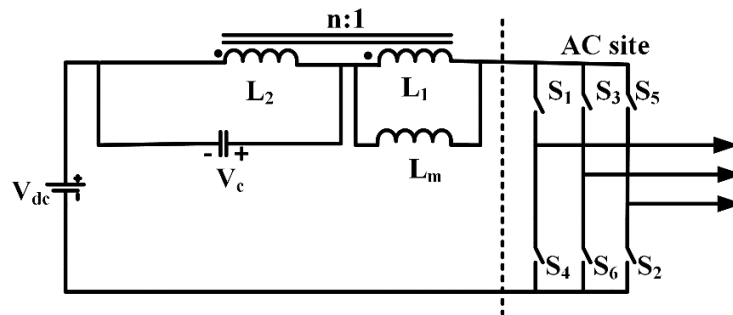


Figure 3. Embedded ZSI [24]

In the first operating condition the time interval for on condition is  $0 \leq t < 0.5D_{ST}T_s$  at that off the off time period is from  $0.5T_s \leq t < 0.5(1 + D_{ST})T_s$ . Under this mode of operation the two diodes  $D_a$  and  $D_b$  as shown in figure, the voltage across the two diodes is  $-V_c$ . By applying Kirchoff's voltage laws (KVL)  $V_i = V_c + V_i$ . As the switches of the inverter are turned on, the inverter output voltage will change to zero voltage. The second operating mode occurs during the time interval of  $0.5D_{ST}T_s \leq t < 0.5(1 + D_{ST})T_s$ . Here the capacitor current can be found out by applying KCL. Therefore, the capital current  $I_c = I_i + I_d$ . Similarly, by applying KVL at the inductor voltage becomes  $V_i = V_i - V_c$ . As soon as diode  $D_b$  becomes forward biased the DC link voltage stood at  $V_{dcmax} = V_c$ . Similarly the load voltage  $V_o = V_{dcmax}$ .

The third operating mode will work between the time in interval of  $0.5(1 - D_{ST})T_s \leq t < T_s$ . In this mode voltage across the capacitor and that of stored energy will increase. Because of the negative voltage add inductor the stored energy and the current will decrease gradually the value of load voltage becomes  $V_o = -V_{dcmax}$ .

### 2.3. Embedded quasi-Z-source inverter

Unlike embedded ZSI, the embedded q-ZSI maintains smaller amount of people for both input current and voltage. In addition to the above advantages, it also makes the input current continuous. Without adding extra element to the input source it is able to draw smooth current from the source without adding other components. As compared to classical q-ZSI, here an extra source is embedded into the system. The basic concept of embedding the DC source will provided the advantages to both q-ZSI as well as embedded topologies. Two modes of operation is possible such as non shoot through state and shoot through state.

Figure 4 shows the embedded q-ZSI under shoot through mode. As observed, the capacitor voltage will be charged to its maximum limit through coupling inductor  $L_1$  and  $L_2$ . During this mode of operation,  $S_1$ – $S_6$  will be turned off mode. Similarly, the non-shoot through mode is shown at Figure 5 where the energy stored at capacitor will be discharged to the output circuit. As shown in Table 1 the voltage stress on the switches of trans-ZSI (T-ZSI) will be high. Again, the boost factor in all the z-source network topology except trans-z-source is less.

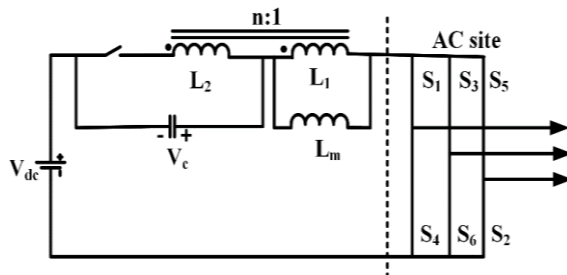


Figure 4. Embedded q-ZSI under shoot through mode

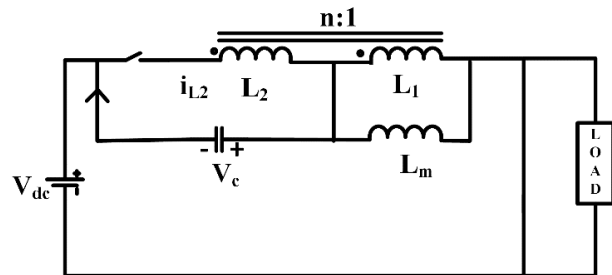


Figure 5. Embedded q-ZSI under non-shoot through mode

Table 1. Comparative analysis of different Z topology network

Z topology network	Boost factor (B)	Switching devices	Capacitors used	Inductor used	Voltage stress on switches
Z-source	$\frac{1}{1-2D}$ where $0 \leq D \leq 0.5$	1	2	2	$\frac{1}{1-2D} v_{in}$
Quasi Z-source	$\frac{1}{1-2D}$ where $0 \leq D \leq 0.5$	1	2	2	$\frac{1}{1-2D} v_{in}$
Embedded Z-source	$\frac{1}{1-2D}$ where $0 \leq D \leq 0.5$	1	2	2	$\frac{1}{1-2D} v_{in}$
Embedded quasi Z-source	$\frac{1}{1-2D}$ where $0 \leq D \leq 0.5$	1	2	2	$\frac{1}{1-2D} (v_1 + v_2)$
Trans Z-source	$\frac{1}{1-(n+1)D}$ where $0 \leq D \leq (n+1)^{-1}$	1	1	Two winding are added	$\frac{n}{1-(n-1)D} v_{in}$

### 3. PROPOSED Z-SOURCE INVERTER APPLICATIONS

In conventional VSI, the inverter output voltage that is from line to line cannot be more than the DC link voltage. In a hybrid EV where the source has been taken from both solar and battery, it is observed that the DC link voltage cannot be made constant throughout the operation. This further requires a DC to DC boost converter in order to boost the DC link voltage so as to maintain the required output at inverter terminal. This methodology increases the complexity of the overall system at the same time reduces the

efficiency and also reliability. Again in the conventional VSI two legs cannot be sorted at the same time of its operation. In order to have a safety operation in the inverter topology, a dead time of 10 microsecond is usually applied in between the two switches of a leg. This leads to increase in the harmonics at the output of the inverter, which for the required for an LC filter to bring down the harmonics into the normal range. A typical ZSI with modification in the control strategy can be used to avoid such type of problem in the VSI. In the proposed model, the ZSI can do the the boost and buck operation in a single stage conversion structure. The dead time is no more required in the proposed ZSI at the same time the output waveforms become more sinusoidal with less electromagnetic interference.

Figure 6 shows the inverter technology with neural network (NN) and battery powered induction motor. In order to achieve firing angle control for different switches feedback loop has been established by tracking the speed of induction motor through offline mode controller. The offline mode of controller consists of four stage conversion of vector distribution and function order estimation. Two dynamic variables such as DC voltage and capacitor voltage (DC link) has been given as feedback to the function order value and vector order distribution parameter. In order to generate six pulse firing pattern the univariate basis function has been transferred into a multivariate basis function. The speed adjustment has been carried out by using network with function. The network function can be a variable predefined with threshold limit.

The output of the offline mode is transferred into a online mode NN where the learning rate as a function of the six switching patterns prepares the learning rule for each model. This learning rule will calculate the network layer along with individual basis function in terms of proportional and integral constant for the PWM converter. The PWM converter upon reading the DC link reference voltage will generate individual gating sequence for six switches. The acceleration and retardation operation of the induction motor will be made proportional to the switching sequence to the converter. The two different mode of operation of the inverter such as shoot through mode and non-shoot shoot through mode can be easily achieve with dynamic behavior of NN is predicting PWM gating sequence.

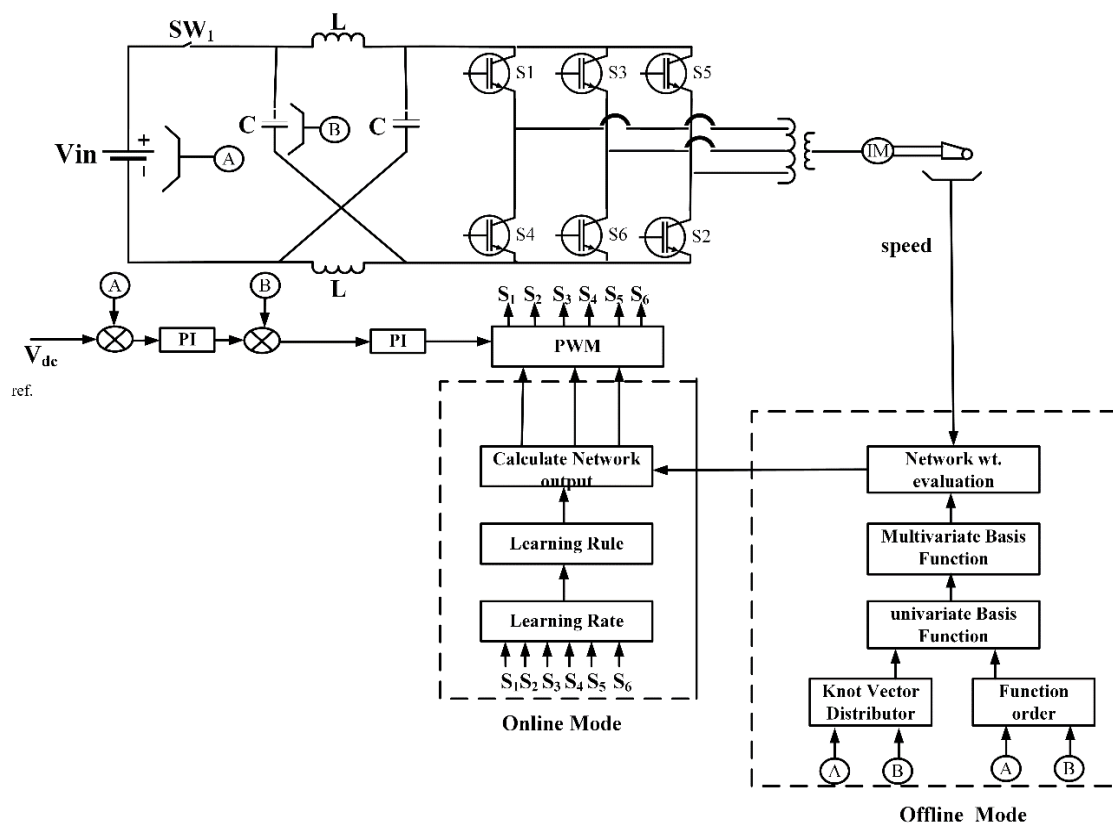


Figure 6. Inverter technology with NN and a battery powered EV

#### 4. RESULTS AND DISCUSSION

In order to investigate the performance of different types of inverter technology with NN and a battery powered EV has been modelled with T-ZSI as shown in Figure 6. Figure 7 shows a detailed hardware setup,

induction motor drive with T-ZSI. Here the induction motor has been taken as a critical load for harmonic investigation and its analysis. The detailed technical parameters of the induction motor and induction motor drive is shown in Tables 2 and 3 respectively.

A MATLAB/Simulink model has been developed with details parameters as shown in Tables 2 and 3 respectively. In order to investigate the robustness of the EV in terms of supplied current and voltage quality an unit step function analysis has also been carried out to T-ZSI through hardware testing. Figure 8(a) represents the DC link capacitor reference voltage maintained at the input of T-ZSI for induction motor drive. Here an average of 250 V has been maintained. The same voltage has also been maintained through the hardware model as shown in Figure 8(b). Here a ripple content of 10% found both in hardware and software. The inverter output voltage was found to be 220 V in MATLAB/Simulink model. However, the same voltage has been observed through the T-ZSI at its output with a magnitude of 228 V. Figures 9(a) and (b) represents both simulations and hardware results of inverter.

Table 2. MATLAB/Simulink induction motor parameter

Sl. No	Parameter	Rating	Remarks
1	Power	186	V-A
2	Voltage ( $V_{RMS}$ )	110	V
3	Frequency	60	Hz
4	Main winding stator resistance	2.02	$\Omega$
5	Leakage inductance	$7.4 \times 10^{-3}$	Henry
6	Mutual inductance	0.1772	Henry
7	Auxiliary winding stator resistance	7.14	$\Omega$
8	Leakage inductance	$8.5 \times 10^{-3}$	Henry
9	Turns ratio	1.18	
10	Main winding rotor resistance	4.12	$\Omega$
11	Leakage inductance	$5.6 \times 10^{-3}$	Henry
12	Inertia	0.0146	Kg-m <sup>2</sup>
13	Friction	0	
14	Pole pair	2	

Table 3. MATLAB/Simulink induction motor drive parameter

Sl. No	Parameter	Rating	Remarks
1	Snubber circuit resistance	10,000	$\Omega$
2	Capacitance	20	n-F
3	Diode on state voltage drop	0.8	V
4	Diode on state resistance	$1 \times 10^{-3}$	$\Omega$
5	DC bus capacitor	$39 \times 10^{-4}$	F
6	Breaking chopper resistance	8	$\Omega$
7	Chopper frequency	4	K-Hz
8	Acceleration voltage	310	V
9	Shift down voltage	300	V

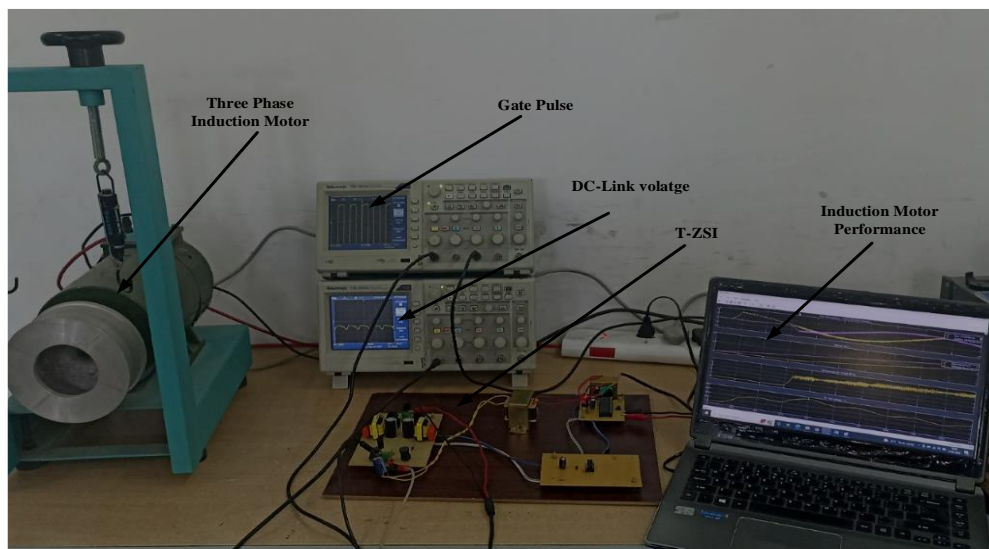


Figure 7. Detailed hardware setup, induction motor drive with T-ZSI



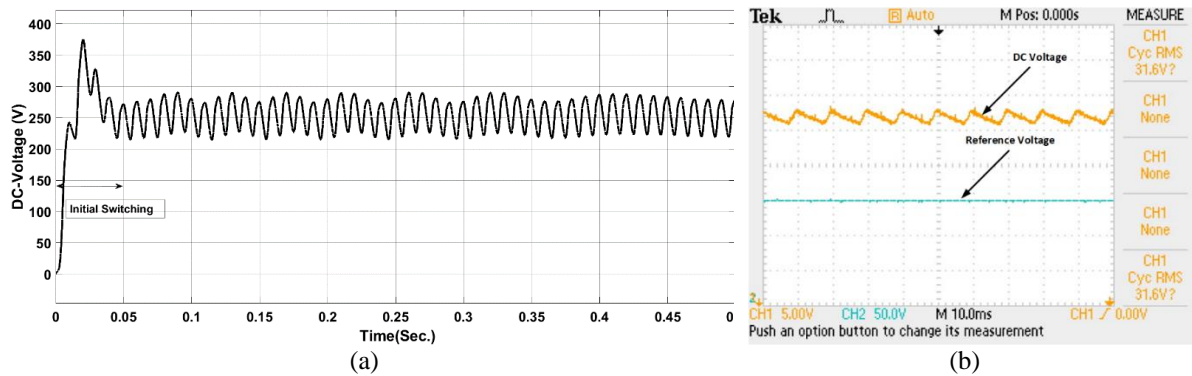


Figure 8. DC reference voltage; (a) DC link capacitance voltage through MATLAB/Simulink and (b) DC link capacitor voltage taken from hardware set up

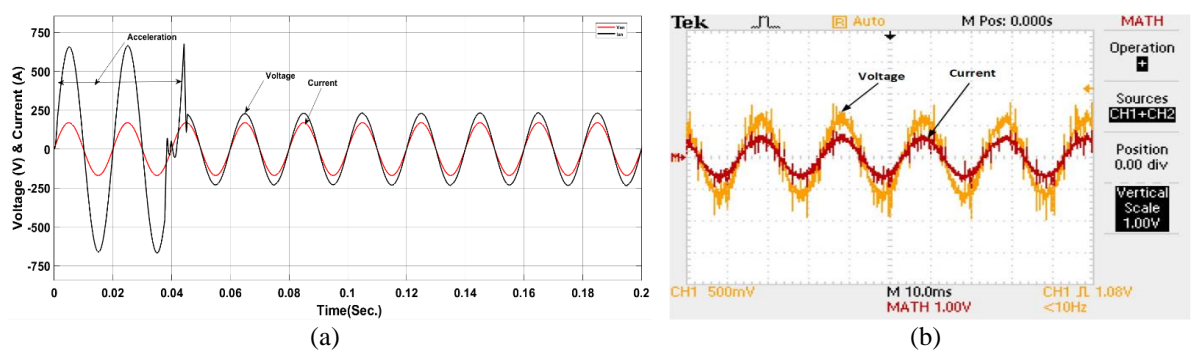


Figure 9. Voltage and current waveform captured using; (a) MATLAB at the input of induction motor and (b) hardware set up at the input of induction motor

A detail total harmonic distortion (THD) comparison of both the hardware and software result is shown in Figure 10. As noticed at Figure 10(a) a total THD of 12.16 Hz is present over one cycle of voltage signal and that off Figure 10(b) the hardware result, despite a THD level of 13.07 Hz. This shows that T-ZSI can achieve more robustness in terms of supplying current and voltage by maintaining required DC link voltage to the induction motor drive circuit without creating much heating effect for the battery. Figure 11 shows the electromagnetic torque developed inside the induction motor.

The DC ripple present in the electromagnetic torque is due to the presence of THD. The electromagnetic torque shows an initial oscillation of magnitude 4 N-m for 0.1 seconds, this is because of the inverter switching action. At about 0.22 seconds a peak has been observed because of closing of the circuit breaker. At about 0.45 seconds the circuit breaker turned off for one voltage source. Hence the complexity of waveform is minimized. Figure 12 shows the main current and auxiliary current of the induction motor. It is observed that auxiliary current is lagging the main current at an angle of 0.3 radians.

Figure 13 shows the step response analysis of the current controller used in the experimental setup for verifying the robustness of the PI controller. Figure 13(a) represents the MATLAB/Simulink step response of the controller. From Figure 13(b), it is observed that a maximum overshoot of 47.82% with risetime of 0.07 sec. having a settling time of 1.07 sec Here it can be concluded that, there is an error of 6% (almost) present in the simulation and the actual results.

Figure 14 shows the triggering sequence for the insulated gate bipolar transistor (IGBT) switch. It is observed that gating sequence follow the NN project sequence patter with a delay of 0.03 micro sec. Similarly Figure 15 represents the transits response of the current controller used in the PWM switching patter generation. A transient time at 0.3 seconds, represents deacceleration of induction motor. It takes almost 0.68 seconds to stabiles the current drawn from the inverter.



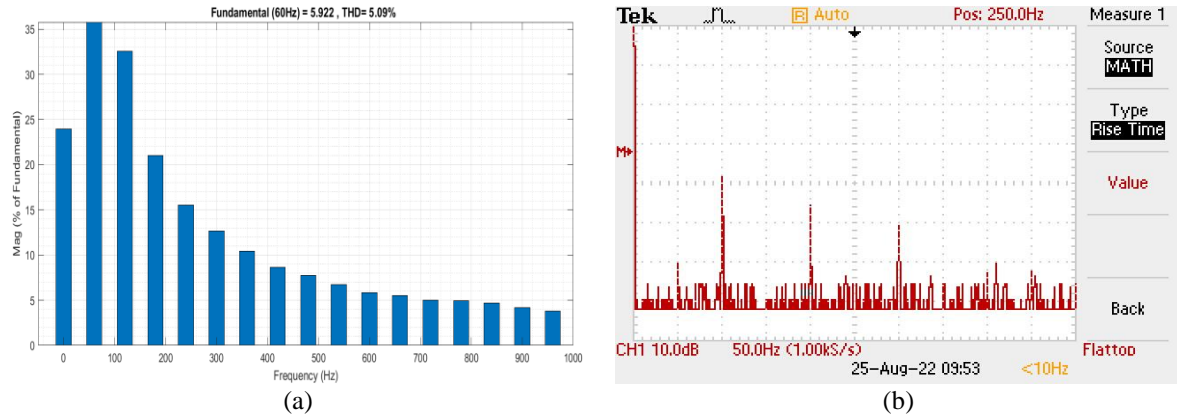


Figure 10. THD analysis using; (a) MATLAB/Simulink and (b) hardware set up

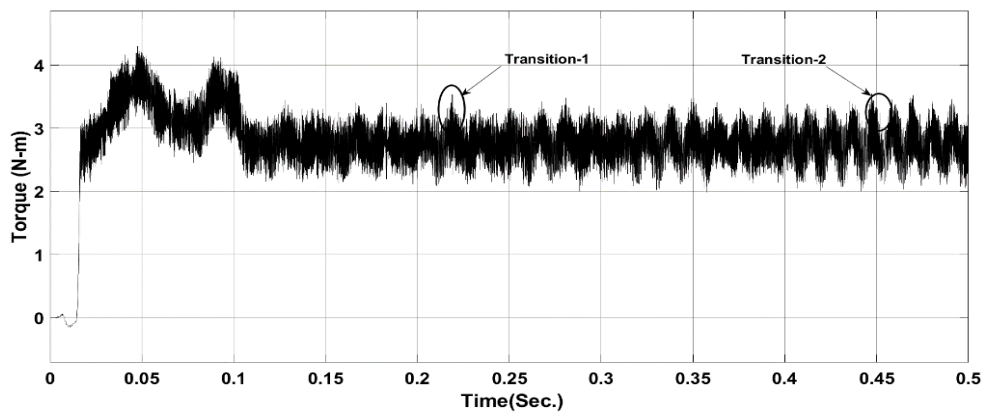


Figure 11. Electromagnetic torque developed inside the induction motor

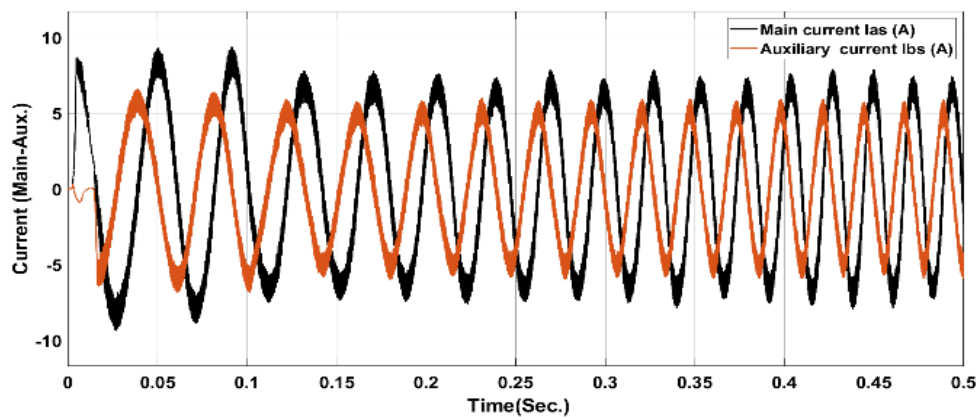


Figure 12. Main current and auxiliary current waveform of the induction motor

Figure 16 shows the NN regression analysis for 70% of training data set (Figure 16(a)) and that of 30% analysis of testing set (Figure 16(b)). A comparison between the two training and testing, the R value is 0.33016. This shows that the error between the two algorithms is almost zero, which depicts that both the algorithm is robust. Figures 17 and 18, represents the training performance and the validation check at each epoch. It is observed that for Figure 18(a), the gradient distribution is initially a smooth step function whereas after 80 epochs a large variation has been observed, this is due to acceleration and retardation of induction motor. All the validation check are factor with zero passing argument for all 172 epochs as presented at Figure 18(b). Similarly, the gradient distribution is almost 35090.3559 at each 172 epochs.

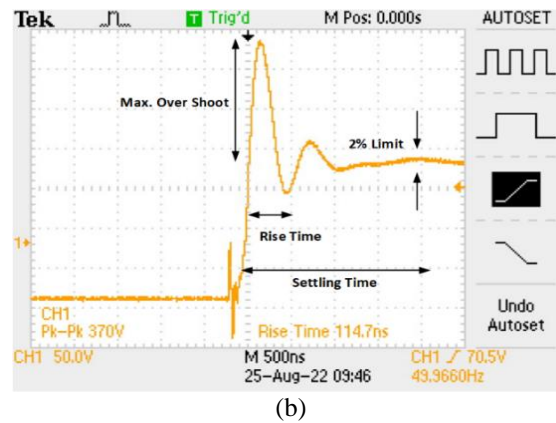
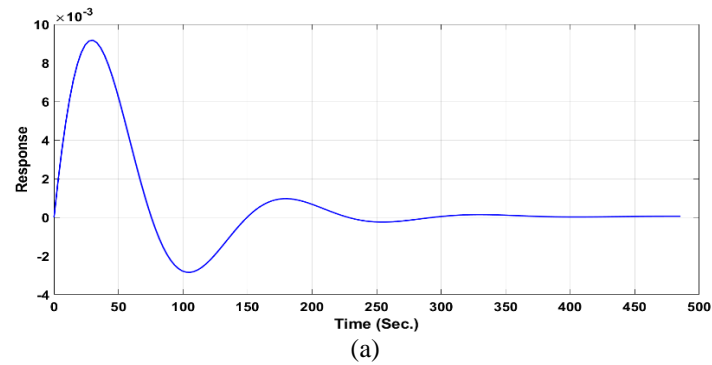


Figure 13. Step response of the current controller; (a) in MATLAB/Simulink and (b) from hardware using trigger mode

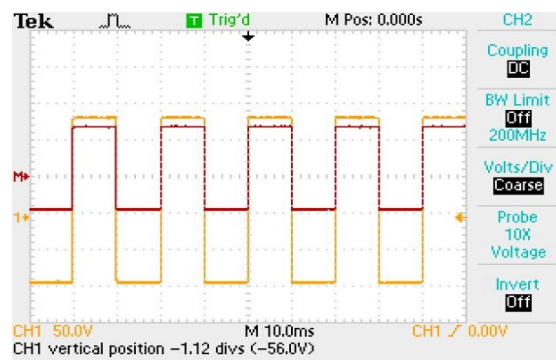


Figure 14. Gate triggering sequence for IGBT

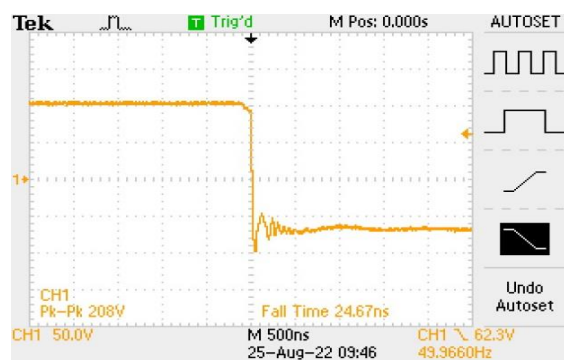


Figure 15. Transient response of the current controller used in PWM switching pattern generation

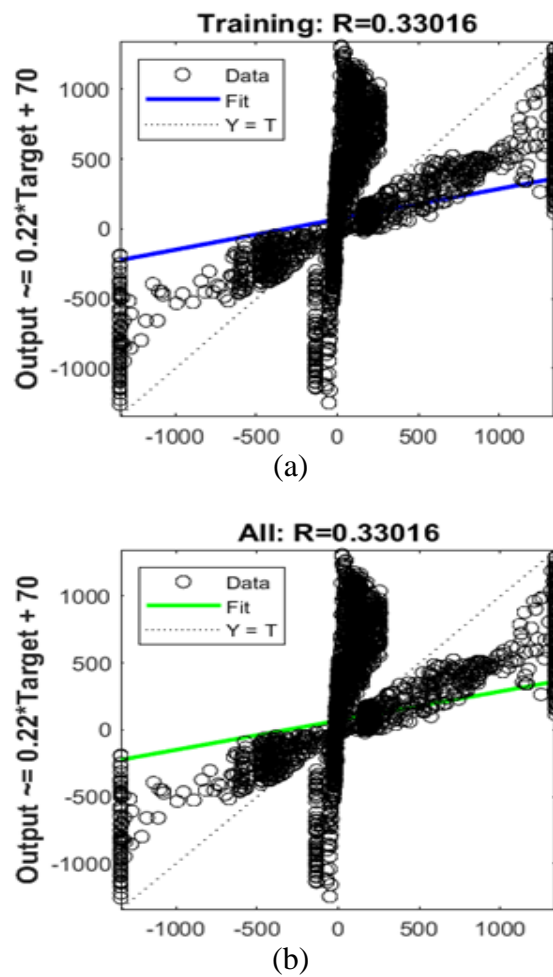


Figure 16. NN-regression analysis for; (a) training set and (b) testing set

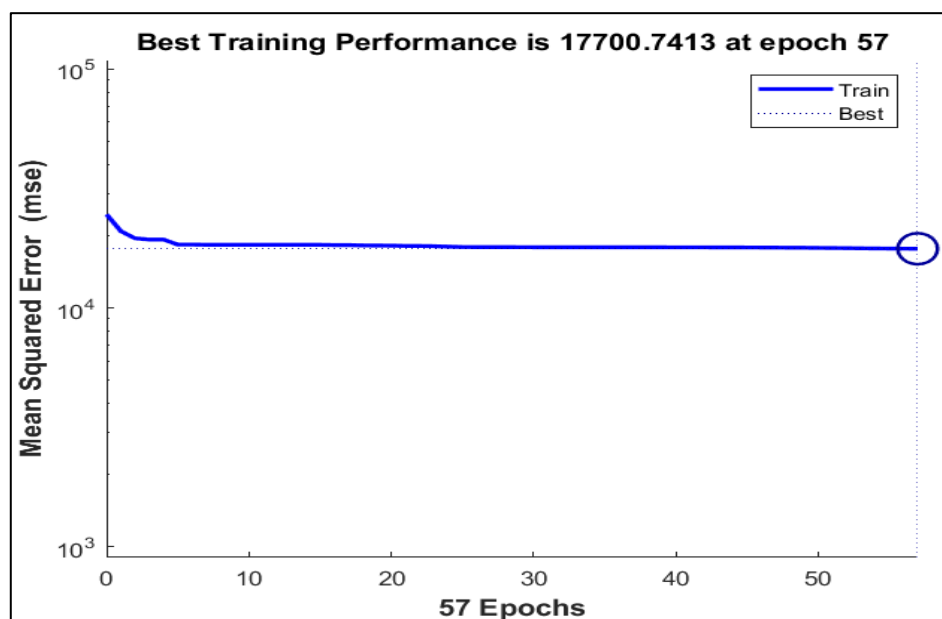


Figure 17. Training performance under neural model analysis

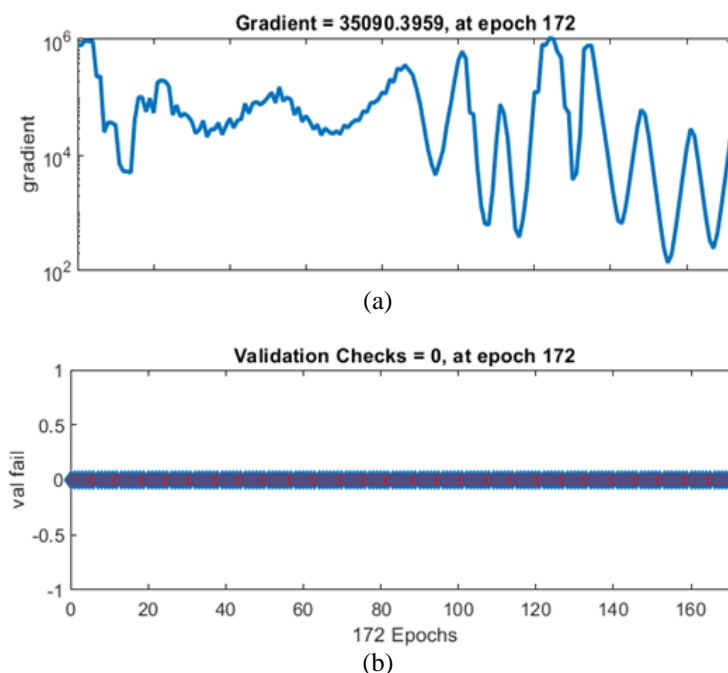


Figure 18. Training performance under neural model analysis (a) gradient analysis and (b) validation check

## 5. CONCLUSION

The paper presents a detailed analysis of different types of ZSI. Application of T-ZSI to the EV has been modelled using MATLAB/Simulink software and the corresponding hardware model has also been developed and verified. The experimental setup (hardware) has been tested for its robustness in terms of two parameters such as: i) a step input response to the current controller and ii) THD along with DC-link capacitor voltage. The result and the experimental analysis present under section four depicts that during acceleration the T-ZSI is providing the required amount of current within 34.67 micro seconds while during retardation process it took approximately 0.03 seconds to stabilize the controller so as to generate the necessary gating sequence for electric motor drive, here referred as induction motor.

The use of NN shows that the induction motor can be well controlled in terms speed and torque by creating multi-dimensional diverse function. It is also notices that the use of NN helps in reducing the THD contribution at the output of the inverter. The shoot through and non-shoot through mode of operation using the NN becomes easier. However, the present research paper does not contribute to the direct torque control of induction motor. This method can be realized in future for achieving independent motor control action in a four motor drive EV system.

## ACKNOWLEDGEMENTS




The author would like to thank school of electrical and electronics engineering, REVA University for providing necessary laboratory facilities for successful completion of the project work. The authors would also like to thank Karnataka State Council for Science and Technology (KSCST), Karnataka for partially funding the project work.

## REFERENCES




- [1] X. Liang, E. Tanyi, and Z. Xin, "Charging electric cars from solar energy," M.S. thesis, Dept. of Elect. Eng., Blekinge Institute of Technology, Karlskrona, Sweden, 2016.
- [2] A. Ul-Haq, C. Cecati, and E. Al-Ammar, "Modeling of a photovoltaic-powered electric vehicle charging station with vehicle-to-grid implementation," *Energies*, vol. 10, no. 1, pp. 1–20, Dec. 2016, doi: 10.3390/en10010004.
- [3] S. M. Shariff, M. S. Alam, F. Ahmad, Y. Rafat, M. S. J. Asghar, and S. Khan, "System design and realization of a solar-powered electric vehicle charging station," *IEEE Systems Journal*, vol. 14, no. 2, pp. 2748–2758, Jun. 2020, doi: 10.1109/JSYST.2019.2931880.
- [4] B. Revathi, A. Ramesh, S. Sivanandhan, T. B. Isha, V. Prakash, and S. G., "Solar charger for electric vehicles," in *2018 International Conference on Emerging Trends and Innovations In Engineering And Technological Research (ICETIETR)*, Jul. 2018, pp. 1–4, doi: 10.1109/ICETIETR.2018.8529129.

- [5] G. P. Shirsat, "Simulation of grid connected EV charging station with renewable energy source," *International Journal of Advanced Trends in Computer Science and Engineering*, vol. 8, no. 1.4, pp. 415–419, Sep. 2019, doi: 10.30534/ijatcse/2019/6481.42019.
- [6] F. Liu, J. Liu, B. Zhang, and H. Zhang, "Fast charging system of electric vehicle (EV) based on hybrid energy storage system," in *2012 Twenty-Seventh Annual IEEE Applied Power Electronics Conference and Exposition (APEC)*, Feb. 2012, pp. 2115–2120, doi: 10.1109/APEC.2012.6166113.
- [7] A. Singh and S. . Shimi, "MATLAB SIMULINK simulation of PV system based on MPPT in variable irradiance with EV battery as load," in *2017 IEEE International Conference on Computational Intelligence and Computing Research (ICIC)*, Dec. 2017, pp. 1–4, doi: 10.1109/ICIC.2017.8524563.
- [8] V. Monteiro, J. G. Pinto, B. Exposto, J. C. Ferreira, and J. L. Afonso, "Smart charging management for electric vehicle battery chargers," in *2014 IEEE Vehicle Power and Propulsion Conference (VPPC)*, Oct. 2014, pp. 1–5, doi: 10.1109/VPPC.2014.7007133.
- [9] J.-S. Moon, J.-H. Lee, I.-Y. Ha, T.-K. Lee, and C.-Y. Won, "An efficient battery charging algorithm based on state-of-charge estimation for electric vehicle," in *2011 International Conference on Electrical Machines and Systems*, Aug. 2011, pp. 1–6, doi: 10.1109/ICEMS.2011.6073783.
- [10] P. Bauer, N. Stembridge, J. Doppler, and P. Kumar, "Battery modeling and fast charging of EV," in *Proceedings of 14th International Power Electronics and Motion Control Conference EPE-PEMC 2010*, Sep. 2010, pp. 39–45, doi: 10.1109/EPEPEMC.2010.5606530.
- [11] B. S. Manju, R. Ramaprabha, and B. L. Mathur, "Modelling and control of standalone solar photovoltaic charging system," in *2011 International Conference on Emerging Trends in Electrical and Computer Technology*, Mar. 2011, pp. 78–81, doi: 10.1109/ICETECT.2011.5760095.
- [12] M. A. Laguado-Serrano, E. A. Luna-Paipa, L. F. Bustos-Marquez, and S. B. Sepulveda-Mora, "Performance comparison between PWM and MPPT charge controllers," *Scientia et Technica*, vol. 24, no. 1, pp. 6–11, Mar. 2019, doi: 10.22517/23447214.20681.
- [13] R. Paul, R. Dash, and S. C. Swain, "Design analysis of current controller for SPV grid connected system through hysteresis CCT," in *2018 International Conference on Applied Electromagnetics, Signal Processing and Communication (AESPC)*, Oct. 2018, pp. 1–6, doi: 10.1109/AESPC44649.2018.9033188.
- [14] S. Mishra and R. K. Viral, "Integration phenomena of renewable energy with contemplation of issues from electricity distribution utility and consumer perspective," in *2021 International Conference on Sustainable Energy and Future Electric Transportation (SEFET)*, Jan. 2021, pp. 1–6, doi: 10.1109/SeFet48154.2021.9375824.
- [15] D. Pattanaik, R. Dash, and S. C. Swain, "A review on solar thermal PV modeling its characteristics," in *2018 International Conference on Applied Electromagnetics, Signal Processing and Communication, AESPC 2018*, Oct. 2018, pp. 1–6, doi: 10.1109/AESPC44649.2018.9033370.
- [16] C. Nsengimana, X. T. Han, and L. Li, "Comparative analysis of reliable, feasible, and low-cost photovoltaic microgrid for a residential load in Rwanda," *International Journal of Photoenergy*, vol. 2020, pp. 1–14, Nov. 2020, doi: 10.1155/2020/8855477.
- [17] D. Pattanaik, R. Dash, and S. C. Swain, "Design analysis of hybrid PSPS with SPV under islanding mode of operation," in *2018 International Conference on Applied Electromagnetics, Signal Processing and Communication (AESPC)*, Oct. 2018, pp. 1–5, doi: 10.1109/AESPC44649.2018.9033342.
- [18] M. J. Khan, A. K. Yadav, and L. Mathew, "Techno economic feasibility analysis of different combinations of PV-wind-diesel-battery hybrid system for telecommunication applications in different cities of Punjab, India," *Renewable and Sustainable Energy Reviews*, vol. 76, pp. 577–607, Sep. 2017, doi: 10.1016/j.rser.2017.03.076.
- [19] S. Mishra, D. Pattanaik, R. Pau, R. Dash, and S. C. Swain, "A review on different types of maximum power point tracking system its application with PR current control technique," in *2018 International Conference on Applied Electromagnetics, Signal Processing and Communication (AESPC)*, Oct. 2018, pp. 1–6, doi: 10.1109/AESPC44649.2018.9033187.
- [20] R. R. Tobias et al., "Design and construction of a solar energy module for optimizing solar energy efficiency," in *2020 IEEE 12th International Conference on Humanoid, Nanotechnology, Information Technology, Communication and Control, Environment, and Management (HNICEM)*, Dec. 2020, pp. 1–6, doi: 10.1109/HNICEM51456.2020.9400127.
- [21] S. C. Swain, A. Gogoi, S. Sharma, R. Dash, and A. Acharya, "Some aspects of fuzzy logic controller for designing MPPT based SPV system," in *2018 International Conference on Recent Innovations in Electrical, Electronics & Communication Engineering (ICRIEECE)*, Jul. 2018, pp. 3357–3361, doi: 10.1109/ICRIEECE44171.2018.9009418.
- [22] M. Bernard and P. Musilek, "Ant-based optimal tuning of PID controllers for load frequency control in power systems," in *2017 IEEE Electrical Power and Energy Conference (EPEC)*, Oct. 2017, pp. 1–6, doi: 10.1109/EPEC.2017.8286152.
- [23] R. Samanbakhsh, P. Koohi, F. M. Ibanez, F. Martin, and V. Terzija, "A Z-source inverter with switched network in the grid-connected applications," *International Journal of Electrical Power & Energy Systems*, vol. 147, pp. 1–13, May 2023, doi: 10.1016/j.ijepes.2022.108819.
- [24] X. Duan, L. Kang, H. Zhou, and Q. Liu, "Multivector model predictive power control with low computational burden for grid-tied quasi-Z-source inverter without weighting factors," *IEEE Transactions on Power Electronics*, vol. 37, no. 10, pp. 11739–11748, Oct. 2022, doi: 10.1109/TPEL.2022.3174303.
- [25] C. Tao, Z. Liu, S. Li, Y. Guo, and L. Wang, "A high-efficiency wireless power transfer system using quasi-Z-source inverter and current-double synchronous rectifier for low-voltage and high-current applications," *IEEE Transactions on Transportation Electrification*, vol. 8, no. 2, pp. 2758–2769, Jun. 2022, doi: 10.1109/TTE.2022.3146426.
- [26] J. P. Kelley, D. A. Wetz, G. K. Turner, and I. Cohen, "Integration of pulsed loads into a Microgrid architecture," in *2013 Abstracts IEEE International Conference on Plasma Science (ICOPS)*, Jun. 2013, pp. 1–1, doi: 10.1109/PLASMA.2013.6633457.




**BIOGRAPHIES OF AUTHORS**

**Manish Bharat**    (Member, IEEE), Assistant Professor, School of Electrical and Electronics Engineering, REVA University, Holds M.E Degree in "Power Electronics and Drives" from Anna University and B.E degree in Electrical and Instrumentation Engineering from Satyabhama University. Currently he is pursuing Ph.D. under Visvesvaraya Technological University (VTU) Belagavi. He has 12 years of Teaching Experience and 2 years of experience in product development. He has 8 Patents published under IPR, under Government of India. He is active member of IET, IAENG and IEEE. He has 12 publications in various journals and conferences. His areas of research include Z source inverter and its topology, EV charging, and DC-DC converters. He can be contacted at email: manishb87@gmail.com.



**ASR Murty**    Retd. Professor, Department of Electrical and Electronics Engineering, Rajarajeswari College of Engineering. He completed his M.Tech. in Electrical Engineering on 1978 from IIT Kanpur and Ph.D. in Electrical Engineering on (1997) from IIT Chennai. He worked in Central Power Research Institute, Bangalore as Scientist Grade V, EO III, EO IV, and joint director used SIMPOW package for power system analysis and developed several tailor made programs in FORTRAN for power system analysis and rendered consultancy services to various electric power utilities. He also handled various subject for U.G and P.G level such as DBMS, Programming languages, unix systems programming, theory of computation, C++, Java, signals and systems, digital signal processing, power system operation and amp; control, electric power utilization in various engineering colleges at UG level as a Professor. He can be contacted at email: asrmurty1954@gmail.com.



**Ritesh Dash**    (Member, IEEE) was born in Bhubaneswar, Odisha, India, in 1989. He received the Ph.D. degree from the School of Electrical Engineering, KIIT University. He is currently working as an Associate Professor at REVA University, Bengaluru. He has a research experience of over ten years and has sound knowledge in the field of artificial intelligence, FACTS, and machine learning. He has published more than 100 numbers of research papers both in international journals and conferences. Earlier, he has also published a book under CRC press. He has also served the Government of India as a Design Engineer, Electrical at WAPCOS Ltd., A Central PSU under Ministry of Water Resources and Ganga Rejuvenation. He has received Madhusudan Memorial Award and the Institutional Award from the Institution of Engineers, India. He is associated with Many International Bodies, such as IEEE, Indian Science Congress, The Institution of Engineers, Solar Energy Society of India, and Carbon Society of India. He can be contacted at email: rdasheee@gmail.com.